Chin. J. Astron. Astrophys. Vol. 7 (2007), No. 5, 693–704
(*http://www.chjaa.org*)

Chinese Journal of
Astronomy and
Astrophysics

X-ray Spectroscopy of Dips of Cir X-1 *

Ya-Juan Lei[1], Fang-Jun Lu[1], Jin-Lu Qu[1], Li-Ming Song[1] and Cheng-Min Zhang[2]

[1] Laboratory for Particle Astrophysics, Institute of High Energy Physics, Chinese Academy of Sciences, Beijing 100049; *leiyj@mail.ihep.ac.cn*
[2] National Astronomical Observatories, Chinese Academy of Sciences, Beijing 100012

Received 2007 January 17; accepted 2007 April 24

Abstract We present X-ray spectral analyses of the low-mass X-ray binary Cir X-1 during X-ray dips, using the *Rossi X-ray Timing Explorer (RXTE)* data. Each dip was divided into several segments, and the spectrum of each segment was fitted with a three-component blackbody model, in which the first two components are affected by partial covering and the third one is unaffected. A Gaussian emission line is also included in the spectral model to represent the Fe Kα line at $\sim$ 6.4 keV. The fitted temperatures of the two partially covered components are about 2 keV and 1 keV, while the uncovered component has a temperature of $\sim$0.5–0.6 keV. The equivalent blackbody emission radius of the hottest component is the smallest and that of the coolest component is the largest. During the dips the fluxes of the two hot components are linearly correlated, while that of the third component does not show any significant variation. The Fe line flux remains constant, within the errors, during the short dips. However, during the long dips the line flux varies significantly and is positively correlated with the fluxes of the two hot components. These results suggest: (1) that the temperature of the X-ray emitting region decreases with radius, (2) that the Fe Kα line emitting region is close to the hot continuum emitting region, and (3) that the size of the Fe line emitting region is larger than that of the obscuring matter causing the short dips but smaller than the region of that causing the long dips.

Key words: stars: individual (Circinus X-1) — stars: neutron — X-rays: stars

1 INTRODUCTION

The X-ray light curves of some low mass X-ray binaries (LMXBs) contain dips, which usually occur near phase zero. In some cases, the dips may be due to disk instability resulting from the rapid removal and replenishment of matter forming the inner part of an optically thick accretion disk (e.g., Belloni et al. 1997; Greiner et al. 1996). However, in most cases, the dips are suggested to be due to absorption of matter passing across the line of sight to the X-ray emitting region (e.g., White et al. 1995). The X-ray spectral evolution during the dips can provide us information about the geometry and physical conditions of these regions in the LMXBs (e.g., Asai et al. 2000; Barnard et al. 2001).

The X-ray spectrum of an LMXB usually includes both a continuum and the 6.4 keV Fe Kα line emission components (e.g., Hirano et al. 1987; White et al. 1986). The continuum emission component has often been described by two different models developed in the 1980's: the Western model and Eastern model. The Western model suggests that Comptonization dominates the spectra, which has the form of a power law with high energy cut-off corresponding to the energy limit of the Comptonizing electrons. However, for bright sources, an additional blackbody component representing the emission from the neutron star (NS) is needed

* Supported by the National Natural Science Foundation of China.

(e.g., White et al. 1988). The Eastern model suggests that every observed spectrum contains two spectral components: a multi-temperature disk blackbody emission from the inner disk and a Comptonized emission provided by the seed photons of the NS (e.g., Mitsuda et al. 1989). It has been claimed that the physical conditions of the emission region can be described by the Eastern model. For example, Done et al. (2002) assumed that there is an intrinsic low energy cut-off in the spectrum at ~ 1 keV due to the lack of low energy seed photons, and that the emission of the NS is probably buried beneath an optically thick boundary layer. As a result, the boundary layer dominates the hard spectrum while the disk dominates the soft energies. More recently, a model was proposed and developed by Church et al. (Church & Bałucińska-Church 1995; Church et al. 1997; Bałucińska-Church et al. 1999), in which two continuum components exist in the dipping LMXBs: a simple blackbody emission from the NS plus a Comptonized emission from an extended accretion disk corona (ADC) above the accretion disk in a "progressive covering" description of absorption. In addition, this model ascribes the dips to the absorption of the emission components by obscuring matter. For example, in X1755–338 and X1624–490, the absorption to the blackbody component is primarily responsible for the dipping (Church & Balucińska-Church 1995, 1996), while in X1658–298 the absorption to the blackbody component is lower than that to the Comptonized component (Oosterbroek et al. 2001). In addition, for Cir X-1, Shirey et al. (1999) used a disk blackbody plus a blackbody and a "progressive covering" to fit the spectra during the dips; Ding et al. (2006a) fitted the dip spectra with two blackbodies plus a "progressive covering" for a long dip of Cir X-1 (also see Brandt et al. 1996).

A common feature in the spectra of LMXBs is the Fe Kα line emission at $6.4 \sim 6.7$ keV, but its origin is still in dispute. White et al. (1986) detected the Fe Kα emission line in five out of six LMXBs, and proposed that the emission line is produced by the recombination of Fe $XXVI$ in the inner ADC. Such a scenario was also suggested by Hirano et al. (1987). The Fe Kα emission of the dipping LMXBs is even more interesting since the dips may provide new clues about the location of the line emitting region. Barnard et al. (2001) proposed that in XB 1323–619 the Fe line at ~ 6.4 keV originates probably in the ADC, while Smale et al. (1993) ascribed the Fe line emission to reflection from the accretion disk itself for Cygnus X-2. Using the *RXTE* data, Shirey et al. (1999) investigated the spectral evolution of Cir X-1 during the dips and found that the Fe line flux is roughly constant during the dip transitions, so suggesting that the Fe Kα emission is produced in the scattering medium.

Dips occur frequently in the light curve of Cir X-1, thus providing a good opportunity to study statistically the structure of X-ray emitting regions and the location of the Fe Kα line. The spectral fits of the data of *ASCA*, *RXTE* and *BeppoSAX* during the dips are consistent with a partial covering model, in which the X-ray emission consists of a bright component undergoing varying absorbing matter and a faint component unaffected by the absorbing matter (e.g., Brandt et al. 1996; Shirey et al. 1999; Iaria et al. 2001). The partial covering is a determinant of the behaviors observed in Cir X-1, and matter at the outer edge of the accretion disk, with an edge-on disk orientation, could explain the partial covering of the spectrum (Brandt et al. 1996). Ding et al. (2006a) studied a long dip of Cir X-1 and concluded that the covering matter exists from the surface of NS to the emitting region of iron line in the accretion disk. However, there are other standpoints, for example, Díaz Trigo et al. (2006) showed that there is no need for partial covering to explain the spectral evolution during the dips with *XMM* data.

Each of these previous studies of the dips of Cir X-1 is usually based on the spectral analysis of a particular dip. Here, we present a statistical study of the spectral evolution of Cir X-1 during various dips hopefully to better constrain the structure of the X-ray emitting regions. The present paper is organized as follows: the observations, spectral models, and data analyses are described in Section 2, the results are given in Section 3, a discussion is in Section 4 and a summary in Section 5.

2 OBSERVATIONS AND ANALYSIS

2.1 Observations and Light Curves

The Proportional Counter Array (PCA) of the *RXTE* consists of five non-imaging, coaligned Xe multiwire proportional counter units (PCUs). It has a field of view of $1^\circ \times 1^\circ$ and a total collecting area of $\sim 6500\,\mathrm{cm}^2$. We used five datasets collected by PCU0 and PCU2 when both of them were working, and detected both long-duration ($> 10^4$ s) and short-duration ($< 10^4$ s) dips in these data (Table 1). Since we are interested in the spectral evolution during dips, we only study the dips with durations $\geq 10^2$ s. We divided each dip into a few segments with each containing enough counts for the spectral analysis. Altogether we examined

Table 1 Selected RXTE Observations of Cir X–1

OBSID	Start Time	Stop Time	Exposure(s)
10122–01–04–00	96–09–20 07:47:01	96–9–20 12:30:13	16992
10122–01–04–02	96–09–21 04:40:02	96–9–21 11:01:13	22871
30080–01–01–000	98–03–03 16:42:14	98–03–03 23:22:07	23993
30081–06–01–000	98–10–05 00:07:41	98–10–05 08:01:07	28406
30081–06–01–01	98–10–04 22:31:54	98–10–04 23:36:14	3860
60024–01–01–00	01–02–28 06:54:03	01–02–28 09:10:15	8172
60024–01–01–01	01–02–28 03:40:03	01–02–28 05:59:15	8352
60024–01–01–02	01–02–28 02:00:41	01–02–28 02:48:15	2854
60024–02–01–03	01–02–28 09:41:03	01–02–28 10:10:15	1752

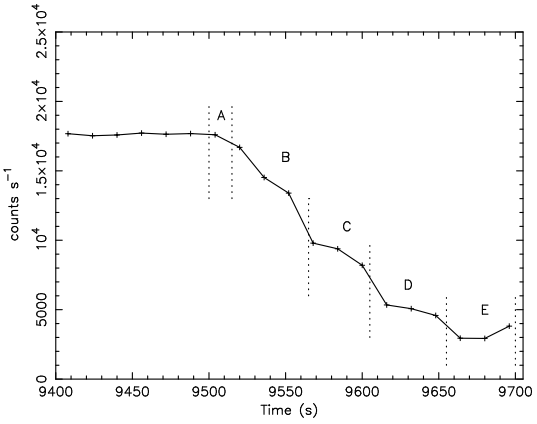

Fig. 1 Typical light curve (16 s bins) around a short-duration dip ($< 10^4$ s) from PCA observations of Cir X-1 (OBSID:30080). For clarity, the errors are not plotted.

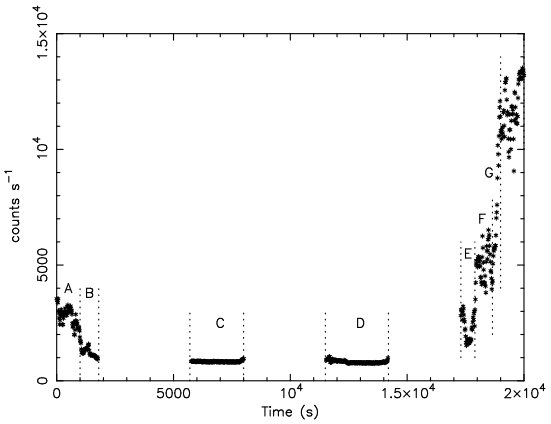

Fig. 2 Typical light curve around a long-duration dip ($> 10^4$ s) from PCA observations of Cir X-1 (OBSID:30081).

three long dips and two short dips, each divided into 5–17 segments studied for their spectral properties. Two typical light curves with the segments marked are shown in Figures 1 and 2.

The data were reduced and analyzed using the *Ftools* software package version v5.2. We filtered the data using the standard *RXTE* criteria, selecting time intervals with the parameters `Elevation_Angles` $> 10^\circ$, `Pointing_Offsets` $< 0.02^\circ$, and the background electron rate `Electron2` < 0.1. Events in the *RXTE* energy range $\sim$ 2.5–25 keV were selected for the spectral analysis. The PCA background subtraction was carried out using the latest versions of the appropriate background models, and a 1% systematic error was

added to the spectra to account for the calibration uncertainties. As usual, the spectral fitting software $XSPEC$ was used.

2.2 Spectral Model

In the literature various spectral models have been used to fit the spectra of Cir X-1 during dips (e.g., Brandt et al. 1996; Shirey et al. 1999; Iaria et al. 2002; Ding et al. 2006a). Brandt et al. (1996) used a model containing two blackbody components and a partial covering. The partial covering can affect the hot component, two or none of them. Shirey et al. (1999) used a model which can be expressed as: $F = [\exp(-\sigma_{\rm ph}N_{\rm H}^{(1)})\exp(-\sigma_{\rm Th}N_{\rm H}^{(1)}) + \exp(-\sigma_{\rm ph}N_{\rm H}^{(2)})f]M$, where F is the observed flux, $\sigma_{\rm ph}$ and $\sigma_{\rm Th}$ are the photoelectric and Thomson cross sections, $N_{\rm H}^{(1)}$ and $N_{\rm H}^{(2)}$ are the effective absorption hydrogen column densities to the bright and faint components, respectively, f is the ratio of the unabsorbed flux of the faint component to the unabsorbed flux of the bright component, and M is the disk blackbody plus blackbody model. Ding et al. (2006a) fitted the dip spectra with the Eastern model and a modified Western model.

However, we find that all the above mentioned spectral models are improper to reveal the physical conditions of the dips. In Brandt et al. (1996) and Ding et al. (2006a), one of the fitted temperatures changes greatly within a dip. For example, the temperature of the disk-blackbody component changes suddenly from $\sim$0.6 keV to $\sim$1.2 keV when the detected flux evolves from the dip bottom to the transition state. Such temperature changes seem unlikely if the dips are mainly due to obscuration, as widely accepted, because the obscuring matter can not change the physical state of the emission region. In the model of Shirey et al. (1999), the residual flux at the bottom of the dips is a fraction of the total emission, while, the hardness-intensity diagram (Fig. 3 in their paper and this paper) shows that the detected spectrum of Cir X-1 is even softer at the lowest flux level than when outside the dip. This means that the residual emission spectrum at dip bottom is intrinsically softer than that out-of-dip spectrum, i.e., it is improper to assume that the residual emission is simply a small fraction of the total emission.

The soft spectrum at the bottom of the dip and the sudden temperature increase of the disk-blackbody component (Ding et al. 2006a) when Cir X-1 moves to the transition state, imply that there exists a weak and soft component which is not affected by the obscuring matter. When there is no dip or when in the transition state, the usually called "NS blackbody emission and disk-blackbody emission" dominate, and so the weak component is difficult to see. When most of the "NS blackbody emission and disk-blackbody emission" are obscured when Cir X-1 is at the bottom of the dips, the contribution of the weak and soft component to the total flux becomes significant or even dominant, and so the detected spectrum at the dip bottom is softer than the out-of-dip spectrum. Such a weak and soft component was also noted by Ding et al. (2006a) but they did not consider it further in the spectral fitting process.

Taking the above facts into account, we use in this paper a spectral model containing three blackbody components and a Gaussian at the energy of Fe Kα line. The first two blackbody components with partial covering are similar to those modelled in Brandt et al. (1996), Shirey et al. (1999) and Ding et al. (2006a), while the additional third component represents the weak and soft emission that are free of partial covering absorption. The expression of our model is: F=wabs[pcfabs*cabs(bbodyrad(1) +bbodyrad(2) +gaussian) +bbodyrad(3)], where wabs represents the photoelectric absorption of the interstellar medium (ISM), pcfabs corresponds to the partial covering photoelectric absorption, cabs accounts for the Compton scattering of the partial covering matter, bbodyrad(1) and bbodyrad(2) represent the continuum emission which is affected by the partial covering, bbodyrad(3) is responsible for the soft faint emission component, and the gaussian accounts for the Fe Kα line emission. As shown later, the fitted parameters by this model are much more reasonable than those in Brandt et al. (1996), Shirey et al. (1999) and Ding et al. (2006a).

In the spectral fitting, the column density of wabs is fixed at 1.8×10^{22} cm^{-2} as determined in the previous work (e.g., Brandt et al. 1996; Iaria et al. 2001), and the column densities of pcfabs and cabs are forced to be identical (Shirey et al. 1999). As shown by the following fitting results (Figs. 4–9, Tables 2–3), such a model gives statistically acceptable fits to both the dip and non-dip spectra, and the obtained parameters look physically reasonable.

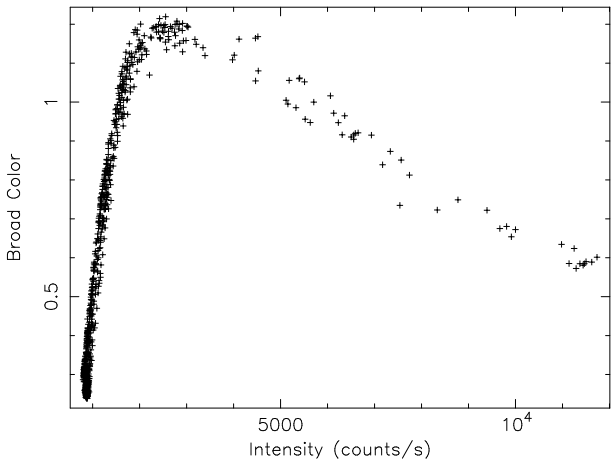

Fig. 3 Hardness-intensity diagram for the data in Fig. 2, intensity is I(2.0–18 keV), the hardness ratio is defined as : I(6.3–18 keV)/I(2.0–6.3 keV). Each point represents 16 s of background-subtracted data from all five PCA detectors (also see, Shirey et al. 1999).

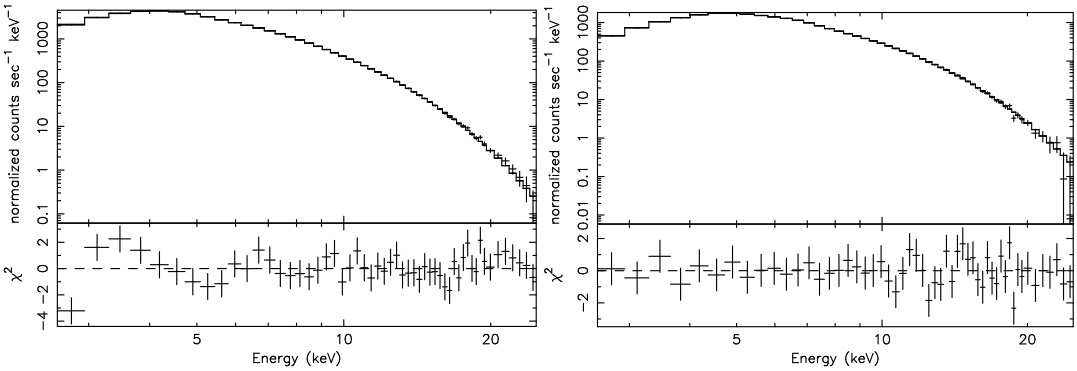

Fig. 4 Left: Typical spectral fit for the dip spectra (spectrum C of OBSID 30080 in Table 2). Right: Typical spectral fit for the non-dip spectra (non-dip data of OBSID 30080), with χ^2 = 55.4 for 54 degrees of freedom.

3 RESULT

The spectra of all the segments have been fitted with the model described in Section 2. Tables 2 and 3 list the spectral fitting results for the segments in OBSIDs 30080 and 30081. In the following we will present our results in various aspects.

3.1 Partial Covering Column Density and Correlations with other Parameters

Brandt et al. (1996) used a partial covering model to fit the spectra before and after the dip transition of Cir X-1, and found a strong Fe Kα edge in the low-state spectra, which indicates that the obscuring matter has a very high column density, $N_{\rm H} > 10^{24}$ cm^{-2}. Shirey et al. (1999) obtained a similar result. Our results show that the hydrogen column density of partial covering absorption is between 10^{22} cm^{-2} and 3.3×10^{24} cm^{-2} (see Fig. 5). The large variation of column density could be due to the partial covering and/or the inhomogeneity of the covering matter.

Table 2 The Fitted Parameters for the Spectra from the OBSID 30080 Dip

Fit Parameters	A	B	C	D	E
$N_{\rm H}^{a}$	1.8(fixed)	1.8(fixed)	1.8(fixed)	1.8(fixed)	1.8(fixed)
$N_{\rm H}^{b}$	$0.0^{+6.3}_{-0.0}$	$2.4^{+0.6}_{-0.3}$	16^{+3}_{-8}	34^{+6}_{-5}	38^{+13}_{-21}
Percentage^{c}	$4.85^{+95.15}_{-4.85}$	95.2(fixed)	$75.0^{+24.4}_{-4.0}$	$89.9^{+2.8}_{-2.9}$	$81.0^{+4.2}_{-5.1}$
kT_1^{d} (keV)	$1.85^{+0.04}_{-0.04}$	$1.87^{+0.05}_{-0.05}$	$1.91^{+0.07}_{-0.08}$	$1.97^{+0.10}_{-0.08}$	$1.89^{+0.08}_{-0.08}$
A_1^{e}	107^{+9}_{-16}	$93.7^{+22.3}_{-8.8}$	$80.1^{+21.4}_{-22.7}$	$61.9^{+23.3}_{-10.7}$	$81.7^{+36.3}_{-23.2}$
flux$_1^{m}$	$1.11^{+0.22}_{-0.16}$	$0.85^{+0.22}_{-0.15}$	$0.49^{+0.21}_{-0.13}$	$0.21^{+23.3}_{-10.7}$	$0.26^{+0.12}_{-0.08}$
$E_{\rm line}^{f}$ (keV)	6.60(fixed)	$6.56^{+0.33}_{-0.28}$	$6.48^{+0.47}_{-0.49}$	6.60(fixed)	$6.64^{+0.34}_{-0.26}$
σ^{g} (keV)	0.5(fixed)	0.5(fixed)	$0.58^{+0.70}_{-0.58}$	$0.36^{+0.21}_{-0.36}$	$0.22^{+0.40}_{-0.22}$
flux^{h}	$12.93^{+5.76}_{-8.71}$	$16.98^{+4.95}_{-9.21}$	$22.33^{+47.80}_{-14.39}$	$14.14^{+8.10}_{-2.95}$	$14.65^{+16.54}_{-4.29}$
kT_2^{i} (keV)	$1.00^{+0.03}_{-0.04}$	$1.03^{+0.01}_{-0.04}$	$1.06^{+0.05}_{-0.12}$	$1.12^{+0.06}_{-0.05}$	$1.08^{+0.06}_{-0.04}$
A_2^{j}	$3.36^{+0.43}_{-0.33}\times10^{3}$	$2.74^{+0.25}_{-0.30}\times10^{3}$	$2.19^{+0.58}_{-0.41}\times10^{3}$	$1.69^{+0.42}_{-0.21}\times10^{3}$	$1.65^{+0.95}_{-0.81}\times10^{3}$
flux$_2^{n}$	$3.92^{+0.43}_{-0.33}$	$2.65^{+0.48}_{-0.28}$	$1.35^{+0.50}_{-0.51}$	$0.57^{+0.17}_{-0.14}$	$0.57^{+0.34}_{-0.28}$
kT_3^{k} (keV)	0.50(fixed)	0.50(fixed)	0.50(fixed)	$0.49^{+0.02}_{-0.02}$	0.50(fixed)
A_3^{l}	$4.60^{+8.38}_{-4.38}\times10^{3}$	$0.0^{+2.93}_{-0.0}\times10^{3}$	$0.02^{+6.47}_{-0.02}\times10^{3}$	$8.45^{+7.08}_{-3.83}\times10^{3}$	$5.32^{+3.87}_{-2.16}\times10^{3}$
flux$_3^{p}$	$0.19^{+0.35}_{-0.18}$	$0.0^{+0.12}_{-0.0}$	$0.0^{+0.28}_{-0.0}$	$0.31^{+0.26}_{-0.14}$	$0.22^{+0.13}_{-0.07}$
$\chi^2\ ({\rm dof})^{p}$	68.63(46)	42.82(46)	35.51(44)	30.46(45)	24.04(44)
χ_ν^{2q}	1.49	0.93	0.81	0.68	0.55

NOTES Model of wabs[pcfabs*cabs(bbodyrad(1)+gaussian+bbodyrad(2))]+wabs*bbodyrad(3) is used. Uncertainties are given at 90% confidence level.

[a] Interstellar column density, in units of 10^{22} cm^{-2}

[b] Partial covering column density, in units of 10^{22} cm^{-2}

[c] Partial covering percentage

[d] Temperature of blackbody(1)

[e] Normalization of blackbody(1)

[m] Flux of blackbody(1) in the 2.0–10.0 keV energy range and in units of photons cm^{-2} s^{-1}

[f] The Gaussian line energy

[g] The Gaussian width

[h] Flux of the gaussian line, in units of 10^{-3} photons cm^{-2} s^{-1}

[i] Temperature of blackbody(2)

[j] Normalization of blackbody(2)

[n] Flux of blackbody(2) in the 2.0–10.0 keV energy range in units of photons cm^{-2} s^{-1}

[k] Temperature of blackbody(3)

[l] Normalization of blackbody(3)

[p] Flux of blackbody(3) in the 2.0–10.0 keV energy range in units of photons cm^{-2} s^{-1}

[p] χ^2 (dof): χ^2: Chi-Squared; dof: degrees of freedom

[q] χ_ν^2: reduced chi-squared: χ^2/dof

Figures 5 and 6 plot the normalizations of the Fe Kα, and of blackbody(1) and blackbody(2) against the partial covering absorption column density. Obviously, the normalization of the Fe Kα line has a positive correlation with $N_{\rm H}$, while the correlations are weak for the normalizations of blackbody(1) and blackbody(2). Since in the spectral fitting the absorption column density and normalization are usually coupled together, we should check whether the correlation between the Fe Kα strength and the absorption column density is real or not. So we derived the ratios of the Fe Kα normalization to the normalizations of blackbody(1) and blackbody(2). As shown in Figures 7 and 8, such coupling-free ratios are also correlated with the absorption column density, indicating that the origin of the Fe emission line is related to the obscuration matter.

Table 3 The Fitted Parameters for Spectra of the OBSID 30081 Dip

Fit Parameters	A	B	C	D	E	F	G
$N_{\rm H}^a$	1.8(fixed)	1.8(fixed)	1.8(fixed)	1.8(fixed)	1.8(fixed)	1.8(fixed)	1.8(fixed)
$N_{\rm H}^b$	43^{+3}_{-4}	81^{+29}_{-42}	325^{+39}_{-53}	247^{+29}_{-40}	44^{+10}_{-8}	23^{+5}_{-4}	13^{+5}_{-8}
Percentage^c	$98.1^{+1.9}_{-9.2}$	$82.9^{+7.6}_{-7.1}$	$89.6^{+2.8}_{-5.3}$	$90.8^{+2.8}_{-5.4}$	$98.0^{+2.0}_{-7.3}$	95.2(fixed)	$55.1^{+44.9}_{-5.5}$
kT_1^d (keV)	$2.14^{+0.04}_{-0.03}$	$2.11^{+0.08}_{-0.07}$	2.20(fixed)	$2.25^{+0.42}_{-0.19}$	$2.11^{+0.05}_{-0.05}$	$2.10^{+0.04}_{-0.04}$	$2.05^{+0.03}_{-0.04}$
A_1^e	$37.3^{+5.0}_{-5.1}$	$31.0^{+45.4}_{-13.9}$	$36.9^{+8.7}_{-5.6}$	$33.5^{+29.9}_{-24.8}$	$37.7^{+9.7}_{-7.4}$	$41.6^{+6.8}_{-5.8}$	$50.0^{+4.2}_{-9.3}$
flux$_1^m$	$0.11^{+0.02}_{-0.02}$	$0.06^{+0.09}_{-0.03}$	$0.00^{+0.00}_{-0.00}$	$0.01^{+0.01}_{-0.01}$	$0.10^{+0.32}_{-0.02}$	$0.23^{+0.04}_{-0.03}$	$0.47^{+0.04}_{-0.09}$
$E_{\rm line}^f$ (keV)	6.60(fixed)	$6.63^{+0.11}_{-0.13}$	$6.56^{+0.06}_{-0.04}$	$6.55^{+0.05}_{-0.05}$	$6.64^{+0.32}_{-0.20}$	$6.65^{+0.27}_{-0.24}$	$6.42^{+0.32}_{-0.40}$
σ^g (keV)	0.50(fixed)	$0.38^{+0.18}_{-0.13}$	$0.20^{+0.12}_{-0.20}$	$0.26^{+0.09}_{-0.15}$	$0.45^{+0.24}_{-0.31}$	$0.39^{+0.28}_{-0.39}$	$0.54^{+0.30}_{-0.43}$
flux^h	$7.36^{+2.88}_{-3.40}$	$8.17^{+4.86}_{-2.60}$	$4.90^{+2.54}_{-2.81}$	$5.64^{+3.94}_{-2.77}$	$14.63^{+3.74}_{-6.14}$	$17.21^{+12.25}_{-7.34}$	$29.31^{+16.96}_{-13.68}$
kT_2^i (keV)	$1.19^{+0.03}_{-0.03}$	$0.84^{+0.13}_{-0.22}$	$1.27^{+0.07}_{-0.07}$	$1.29^{+0.13}_{-0.08}$	$1.21^{+0.06}_{-0.05}$	$1.17^{+0.03}_{-0.03}$	$1.12^{+0.02}_{-0.03}$
$A_2^j \times 10^3$	$0.89^{+0.19}_{-0.15}$	$2.13^{+4.86}_{-1.35}$	$4.11^{+3.31}_{-1.73}$	$2.15^{+1.39}_{-1.09}$	$0.68^{+0.50}_{-0.17}$	$1.16^{+0.30}_{-0.26}$	$1.33^{+0.34}_{-0.46}$
flux$_2^n$ (keV)	$0.23^{+0.05}_{-0.04}$	$0.12^{+0.26}_{-0.07}$	$0.09^{+0.07}_{-0.05}$	$0.09^{+0.05}_{-0.04}$	$0.17^{+0.13}_{-0.08}$	$0.61^{+0.16}_{-0.16}$	$1.40^{+0.35}_{-0.47}$
kT_3^k (keV)	$0.58^{+0.02}_{-0.02}$	$0.54^{+0.07}_{-0.07}$	$0.53^{+0.01}_{-0.02}$	$0.51^{+0.03}_{-0.01}$	$0.54^{+0.02}_{-0.02}$	$0.48^{+0.11}_{-0.09}$	0.50(fixed)
$A_3^l \times 10^3$	$3.61^{+0.70}_{-0.62}$	$4.11^{+2.51}_{-1.57}$	$4.71^{+1.06}_{-0.71}$	$5.33^{+0.97}_{-0.54}$	$4.32^{+1.23}_{-0.91}$	$6.75^{+18.16}_{-4.44}$	$0.0^{+6.85}_{-0.0}$
flux$_3^p$	$0.35^{+0.06}_{-0.06}$	$0.26^{+0.15}_{-0.08}$	$0.28^{+0.03}_{-0.04}$	$0.26^{+0.05}_{-0.05}$	$0.28^{+0.08}_{-0.06}$	$0.22^{+0.60}_{-0.16}$	$0.0^{+0.23}_{-0.0}$
χ^2 (dof)^p	17.68(45)	20.32(43)	23.32(44)	21.17(43)	15.54(43)	18.28(44)	18.45(44)
χ^{2q}_ν	0.39	0.47	0.53	0.49	0.36	0.42	0.42

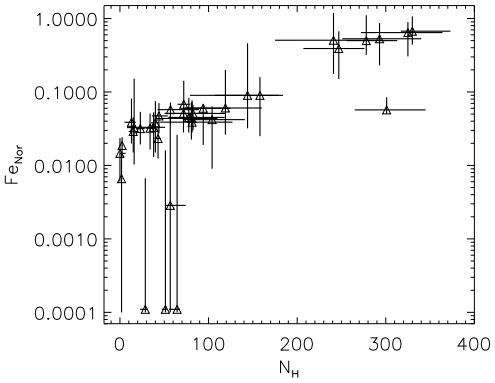

Fig. 5 Normalization of Fe line plotted against $N_{\rm H}$ (in units of 10^{22} cm^{-2}), an obvious correlation can be seen.

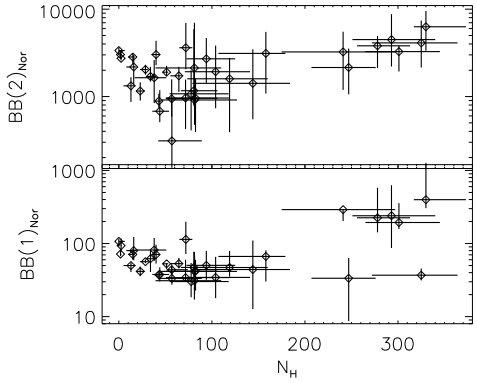

Fig. 6 Normalizations of blackbody(1) (bottom) and blackbody(2) (top) plotted against $N_{\rm H}$. No correlation is seen in either.

3.2 Temperatures and Sizes of Emission Regions

For every dip, the temperature of blackbody(1) is about 2 keV and that of blackbody(2) is about 1 keV, which is consistent with the results of Shirey et al. (1999) with *RXTE*. The temperature of blackbody(3), unaffected by the partial covering, is about 0.5∼0.6 keV, which is consistent with the result of Brandt et al. (1996) with *ASCA*. The almost constant values of the temperature also show that the choice of a three-blackbody-component spectral model is proper.

The distance to Cir X-1 is about 6–10 kpc (e.g., Stewart et al. 1991; Goss & Mebold 1977), so we adopt a value of 8 kpc in converting the blackbody normalization to the radius. The obtained radii of blackbody(1)

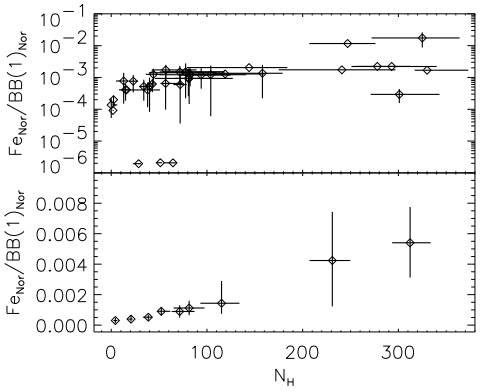

Fig. 7 Ratio of the normalization of Fe line to that of blackbody(1) plotted against $N_{\rm H}$. The bottom panel is a four-point binned plot of the top one. A positive correlation can be seen.

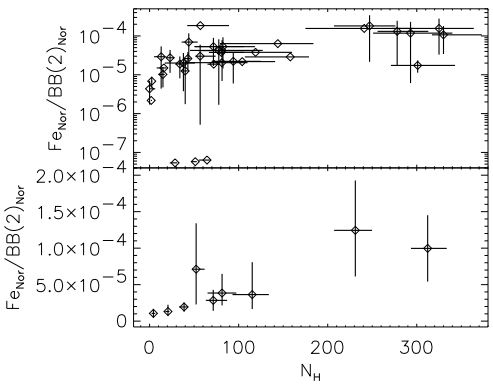

Fig. 8 Same as Fig. 7, but with blackbody(2) substituted for blackbody(1).

(blackbody(2)) are mostly the range of 4–7 km (16–30 km). As for the blackbody(3), its radius generally lies in the range 30–50 km. Since the typical radius of an NS is 10 km, blackbody(1) may come from some hot regions near/on the NS surface, while blackbody(2) and blackbody(3) are perhaps from the inner and outer disk, respectively.

3.3 Flux and Flux Correlations

In Figure 9 we plot the fluxes of blackbody(2) and blackbody(3) against the flux of blackbody(1). A strong correlation is seen between the fluxes of blackbody(1) and blackbody(2) is found, with a correlation coefficient $0.98^{+0.02}_{-0.04}$. However, this plot and further investigations have not shown any sign of a correlation between the flux of blackbody(3) and that of either blackbody(1) or blackbody(2).

We now show that the linear correlation between the fluxes of blackbody(1) and blackbody(2) is intrinsic and not a spurious appearance due to the spectral fitting. In the spectral fitting, blackbody(1) and blackbody(2) are all coupled with the partial covering. When the partial covering column density (and/or covering fraction) is somehow overestimated, the normalizations of the two components will be in turn higher than the real values, and vice versa. Then the two normalizations will show an artificial positive correlation. However, the fluxes plotted in Figure 9 are the absorbed ones (corresponding to the observed fluxes), in which the model coupling effect is eliminated. Therefore, the linear correlation shown in Figure 9 is reliable.

The flux correlation between blackbody(1) and blackbody(2) implies that the two components are usually obscured simultaneously. So their emission regions are probably very close to each other. This is wholly consistent with the conclusions we draw from the equivalent emitting radii in the previous section.

3.4 Fe Line Flux and its Correlations with Continuum Components

Figure 10 plots the Fe line flux versus the fluxes of the continuum components. It is found that the Fe line flux trends increase with increasing fluxes of blackbody(1) and blackbody(2), while there is no clear correlation between it and that of blackbody(3). Since the fluxes for both the line and continuum emissions are mainly due to the obscuration of partial covering matter, the correlation suggests that the region of Fe line emission is close to the hot regions that emit blackbody(1) and blackbody(2).

We further divided the dips into long and short dips, and investigated these correlations for the two classes separately. In Figure 11 for the long dips, the Fe line flux now shows even better correlations with the fluxes of blackbody(1) and blackbody(2). In contrast, Figure 12 for the short dips, now shows no such correlations, in agreement with the results of Shirey et al. (1999). As in Figure 9 for all dips, there is no correlation between the fluxes of the Fe line and blackbody(3) when the long and short dips are separately

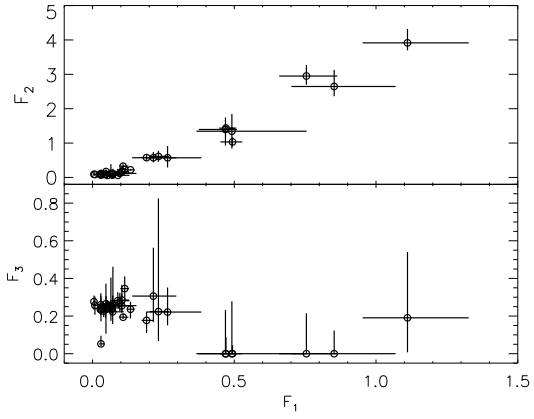

Fig. 9 Flux (in units of photons $cm^{-2}\,s^{-1}$) of blackbody(1) plotted against that of blackbody(2) (top panel) and blackbody(3) (bottom panel). The top panel clearly shows a linear correlation, while no significant relationship is revealed in the bottom panel.

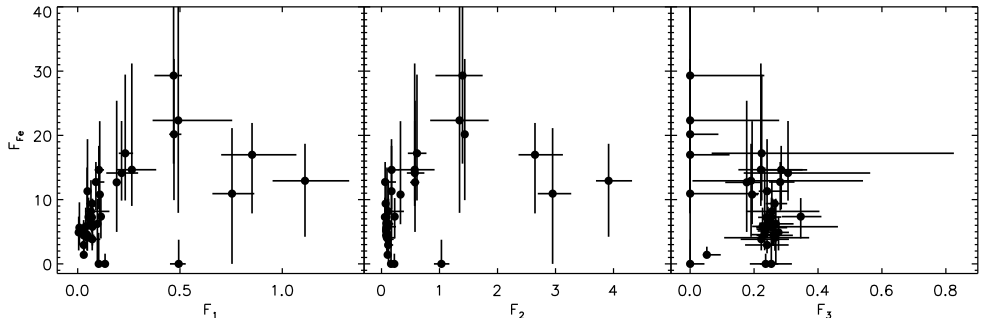

Fig. 10 Fe line flux (in units of 10^{-3} photons $cm^{-2}\,s^{-1}$) plotted against the flux of blackbody(1) (left), blackbody(2) (middle) and blackbody(3) (right), for all the chosen dips (10122-dip1, 30081, 60024, 10122-dip2, 30080).

considered. These results show that the emitting region of the Fe line is smaller than that of the obscuration matter causing the long dips but larger than that causing the short dips.

4 DISCUSSION

The binary system of Cir X-1 has a highly eccentric orbit. Possibly, the NS may be occulted by the outer layers of its companion atmosphere when the stars are close to the periastron. The high eccentricity of the orbit might produce large tidal interactions at this phase, which may in turn expand and/or deform the accretion stream, or may form a bulge in the outer accretion disk. The excess matter may impact on the observed emission of the X-ray source, producing a partial covering of the energy spectrum of the source (e.g., Inoue 1989; Iaria et al. 2001).

The Fe Kα line emission at 6.4$\sim$6.7 keV is a common feature in LMXBs, and its origin has been an interesting topic. Generally, there are four possible sites for the Fe Kα emissions: the accretion disk, the ADC, the source itself, and the scattering medium (e.g., Smale et al. 1993; Shirey et al. 1999; Asai et al. 2000). The observed strong broad line at 6.4$\sim$6.7 keV is generally interpreted as arising from the ADC and the illuminated outer disk (e.g., White et al. 1985; Hirano et al. 1987; Asai et al. 2000), but it is difficult to observe both the line intensity and line width in such a corona.

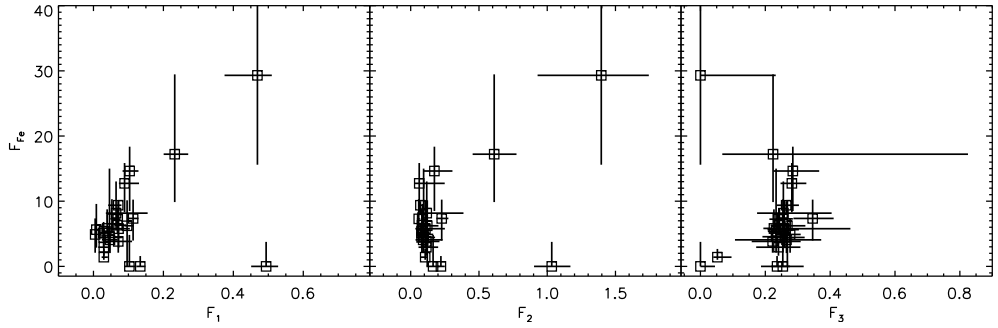

Fig. 11 Same to Fig. 10, but for the long dips (10122-dip1, 30081, 60024). The left and middle panels show a correlation, and not the right one.

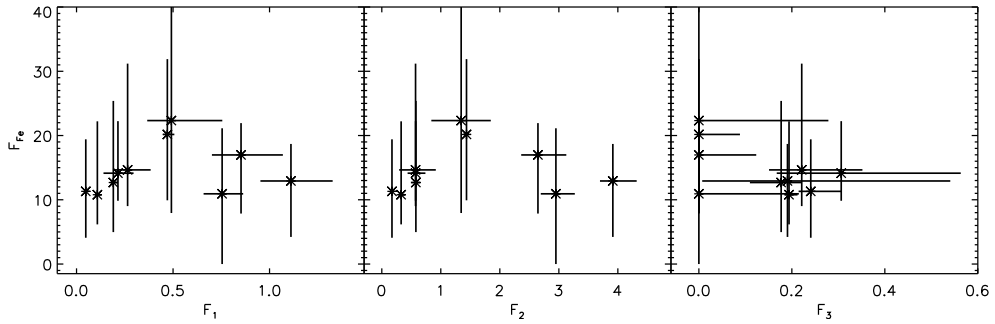

Fig. 12 Same to Fig. 10, but for the short dips (10122-dip2, 30080). The Fe line flux is almost unchanged within the errors, regardless of any of the continuum spectrum fluxes.

For Cir X-1, the results of Shirey et al. (1999) show that the Fe Kα line flux is constant and is associated with the faint component during short dips, implying that the Fe Kα comes from the scattering medium far away from the central region. After investigating the long dips of Cir X-1, Ding et al. (2006a,b) proposed that the Fe line emission is from the disk. Our results show that the flux of this line emission changes obviously during the long dips (see OBSID 30081 in Table 3) and is positively correlated with the fluxes of blackbody(1) and blackbody(2). This implies that the line could not be associated with the soft component unaffected by the partial covering, and instead, it is affected by the partial covering and could come from the region close to the central object.

For the short dips, our result shows that the flux of the Fe emission line is almost constant. There are two possible interpretations for this constant emission: (1) for the short dips the obscuring matter could be of a small size, and (2) the obscuring matter lies inward of the Fe line emission material in the accretion disk. On the other hand, according to the fact that the normalization of the Fe line is positively correlated with $N_{\rm H}$ (see Fig. 5), we also considered that the Fe line could come from the accreting matter, which suggests that the Fe line strength could be related to the mass accretion rate. Dong et al. (2004) showed that the equivalent width of the Fe line was associated with the column density, implying that the line could come from the cold matter invoked in an absorbed model for the active galactic nuclei NGC 2110 and NGC 7582. However, Asai et al. (2000) analyzed the Fe Kα emission lines in the spectra of 20 LMXBs using *ASCA* data, and found that the centroid energies of the Fe lines are almost independent of the source luminosity, nor does the detected equivalent width of the line show any clear correlation with the source category. Although the physical parameters that distinguish these categories have not been figured out, the inclination angle, the mass accretion rate and the stellar magnetic field must be the most relevant quantities.

Thus, Asai et al. (2000) proposed that these parameters may not play a key role in determining the Fe line strength. Unlike the conclusions of Asai et al. (2000), our results favor the statement that the Fe emission line could be correlated with the accreting matter and come from the inner accretion disk.

Nevertheless, we also took note of the Fe emission line in other objects. For some black hole candidates, there is evidence that the observed Fe Kα line originates in the the innermost part of the accretion disk, close to the black hole (e.g., Fabian et al. 1989; Cui et al. 1998; Zycki et al. 1999). In addition, for AGNs, the higher resolution spectra available with the *ASCA* appear to indicate that the line profiles are broad and asymmetrically skewed to lower energies, which is interpreted as evidence that the bulk of the line emission originate from the inner accretion disk around the massive black hole (Nandra et al. 1997; Reynolds & Begelman 1997). Nandra et al. (2000) presented a spectral analysis of the Seyfert 1 galaxy NGC 7469 with *RXTE,* and found a significant correlation between the 2–10 keV flux and the 6.4 keV Fe Kα line, suggesting that the line emission comes from very close to the central regions. Our results imply that the Fe line emission region in the accretion disk of an X-ray binary may be at the same relative location as in an AGN.

5 CONCLUSIONS

In this paper, we analyzed the X-ray dip spectra of Cir X-1. The spectra can be well fitted with two blackbody components with partial covering plus a third blackbody which is unaffected by partial covering. According to the spectral fitting results, the equivalent blackbody emission radii of the first (T $\sim$2 keV), second (T $\sim$1 keV) and third (T = 0.5 $\sim$0.6 keV) component are, respectively, 4–7 km, 16–30 km and 30–50 km. The fluxes of the first and second components are closely correlated, indicating that they both represent emission from the inner regions. The emitting region of the coolest component (3rd) might come from the outer accretion disk.

A 6.4–6.7 keV Fe emission line was detected in the dip spectra. During the long dips, the Fe line flux and fluxes of the first and second components are correlated, while there is no significant correlation between the Fe line flux and the flux of the third component, suggesting the Fe emission line comes from a region very close to the central object and is affected by the covering matter. During the short dips, the Fe line flux is almost constant, within the errors, for all continuum spectra fluxes, which might be due to the fact that the line emission region is in the outward of the obscuring matter or the size of the obscuring matter is much smaller than the Fe line emitting region.

Acknowledgements We would like to thank T. P. Li and S. N. Zhang for useful discussions. This research has made use of data obtained through the High Energy Astrophysics Science Archive Research Center Online Service, provided by the NASA/Goddard Space Flight Center. We acknowledge the *RXTE* data teams at NASA/GSFC for their help. This work is subsidized by the Special Funds for Major State Basic Research Projects and by the National Natural Science Foundation of China (10573017, 10273010, 10473010 and 10773017). We are very grateful for the critic comments from the anonymous referee that greatly improved the paper.

References

Asai K., Dotani T., Nagase F. et al., 2000, ApJS, 131, 571
Barnard R., Balucińska-Church M., Smale A. P. et al., 2001, A&A, 380, 494
Bałucińska-Church M., Church M. J., Oosterbroek T. et al., 1999, A&A, 349, 495
Belloni T., Mendez M., King A. R. et al., 1997, ApJ, 479, L145
Brandt W. N., Fabian A. C., Dotani T. et al., 1996, MNRAS, 283, 1071
Church M. J., Balucinska-Church M., 1995, A&A, 300, 441
Church M. J., Balucińska-Church M., 1996, Memorie della Societa Astronomica Italiana, 67, 395
Church M. J., Dotani T., Balucinska-Church M. et al., 1997, ApJ, 491, 388
Cui W., Ebisawa K., Dotani T. et al., 1998, ApJ, 493, L75
Díaz Trigo M., Parmar A. N., Boirin L. et al., 2006, A&A, 445, 179
Ding G. Q., Qu J. L., Li T. P., 2006a, AJ, 131, 1693
Ding G. Q., Zhang S. N., Li T. P. et al., 2006b, ApJ, 645, 576
Done C., Życki P. T., Smith D. A., 2002, MNRAS, 331, 453

Dong H., Xue S. J., Li C. et al., 2004, Chin. J. Astron. Astrophys. (ChJAA), 4, 427
Fabian A. C., Rees M. J., Stella L. et al., 1989, MNRAS, 238, 729
Goss W. M., Mebold U., 1977, MNRAS, 181, 255
Greiner J., Morgan E. H., Remillard R. A., 1996, ApJ, 473, L107
Hirano T., Hayakawa S., Nagase F. et al., 1987, PASJ, 39, 619
Iaria R., Di Salvo T., Burderi L. et al., 2001, ApJ, 561, 321
Iaria R., Di Salvo T., Robba N. R. et al., 2002, ApJ, 567, 503
Inoue H., 1989, ESA SP-296: Two Topics in X-Ray Astronomy, Vol. 1: X-Ray Binaries. Vol. 2: AGN and the X-Ray Background, p.109
Mitsuda K., Inoue H., Nakamura N., Tanaka Y., 1989, PASJ, 41, 97
Nandra K., Le T., George I. M. et al., 2000, ApJ, 544, 734
Nandra K., Mushotzky R. F., Yaqoob T. et al., 1997, MNRAS, 284, L7
Oosterbroek T., Parmar A. N., Sidoli L. et al., 2001, A&A, 376, 532
Reynolds C. S., Begelman M. C., 1997, ApJ, 488, 109
Shirey R. E., Levine A. M., Bradt H. V., 1999, ApJ, 524, 1048
Smale A. P. et al., 1993, ApJ, 410, 796
Stewart R. T., Nelson G. J., Penninx W. et al., 1991, MNRAS, 253, 212
White N., Nagase F., Parmar A. N., 1995, in X-ray Binaries, ed. W. G. H. Lewin J. van Paradijs, E. P. J. van den Heuvel, Cambridge: Cambridge Univ. Press, p.1
White N. E., Peacock A., Hasinger G. et al., 1986, MNRAS, 218, 129
White N. E., Peacock A., Taylor B. G., 1985, ApJ, 296, 475
White N. E., Stella L., Parmar A. N., 1988, ApJ, 324, 363
Zycki P. T., Done C., Smith D. A., 1999, MNRAS, 305, 231